

A phase separation in diluted Laponite suspensions: evidence of *empty liquid* and *equilibrium gel* states

Barbara Ruzicka¹, Emanuela Zaccarelli², Laura Zulian³, Roberta Angelini¹, Michael

Sztucki⁴, Abdellatif Moussaid⁴, Teyencheri Narayanan⁴, Francesco Sciortino²

¹ *CNR-IPCF and Dipartimento di Fisica, Università di Roma La Sapienza, Piazzale A. Moro 2, I-00185, Rome, Italy.*

² *CNR-ISC and Dipartimento di Fisica, Università di Roma La Sapienza, Piazzale A. Moro 2, I-00185, Rome, Italy.*

³ *CNR-ISMAL via Bassini 15, 20133 Milan, Italy.*

⁴ *European Synchrotron Radiation Facility, B.P. 220 F-38043 Grenoble, Cedex France.*

(Dated: December 2, 2024)

The relevance of anisotropic interactions in colloidal systems has recently emerged in the context of rational design of novel soft materials. Theoretical studies have predicted the possibility of a gas-liquid phase separation confined at low densities and the formation of empty liquids and equilibrium gels in low-valence systems. Here we provide experimental evidence of this scenario in Laponite, a complex colloidal clay with discotic shape and anisotropic interactions. We also report simulations of a patchy model for Laponite platelets, able to reproduce the observed experimental phase diagram and structural properties, confirming the crucial role of the reduced valence.

Patchy colloids [1, 2] are the novel building blocks of a bottom-up approach toward a rational design of self-assembled materials. The novelty of these particles resides in their intrinsic anisotropy, implemented either in shape or in the inter-particle interaction. Recent developments in the synthesis of colloids of different shapes, patterns and functionalities [1] suggest that spontaneously self-assembled bulk materials with pre-defined properties can become feasible in the near future [3–7]. The possibility of tuning the interaction anisotropy will make possible to recreate the molecular world at the nano- and micro-scale (a case with tremendous technological applications) as well as to generate novel unconventional phases, both ordered and disordered. Recent theoretical studies [8], supported by numerical simulations [9], suggest, for example, that the phase-diagram can be significantly altered by limiting the particle coordination number (valence). New concepts such as empty liquids [8] (i.e. liquid states with vanishing density) and equilibrium gels [9–11] (i.e. arrested networks of bonded particles, which do not require an underlying phase separation to form [12]) have emerged. So far, no experimental evidence of these predictions, specific of limited-valence systems, has been provided.

In this work we describe the first experimental realization of the empty liquid scenario in a colloidal suspension. We study Laponite, an industrial synthetic clay made of nanometer-sized discotic platelets with positive charges on the plates and negative ones on the rims. The particle shape and the inhomogeneous charge distribution generate a highly anisotropic interaction potential between the discs. Similarly to other colloidal clays [13, 14], Laponite has technological applications in cleansers, surface coatings, ceramic glazes, personal care and cosmetic products, including shampoos and sunscreens [15]. It is characterized by a very rich, but controversial [15–19], phase diagram including disordered (gels and glasses) and ordered (nematic) phases, on varying colloidal vol-

ume fraction, at fixed ionic strength. The most debated region is the low concentration one (weight concentration $C_w \leq 2.0\%$), where the system ages very slowly up to a final non-ergodic state [18, 19]. This low concentration region is further investigated in this work, extending the observation time to time-scales significantly longer than the previous ones. We discover that, despite samples appear to be arrested on the second time scale (as probed by dynamic light scattering [18, 19]), a significant evolution takes place on the year timescale. Samples indeed undergo an extremely slow, but clear phase separation process into clay-rich and clay-poor phases that are the colloidal analog of gas-liquid phase separation. Spectacularly the phase separation terminates at a finite *but very low* clay concentration, above which the samples remain in a homogeneous arrested state. These features of the phase diagram are strikingly similar to those predicted in simple models of patchy particles [8], suggesting that Laponite forms an (arrested) empty liquid at very low concentrations. Differently from gels generated by depletion interactions [12, 20] or from molecular glass-formers [21], where arrest occurs after the phase separation process has generated high-density fluctuation regions, here phase separation takes place in a sample which is already a gel. Through a very slow rearrangement, the system can thus explore the bottom of its free-energy landscape, finally reaching a stable minimum which corresponds to an equilibrium gel, i.e. a disordered solid.

Fig. 1A-C shows photographs of the temporal evolution of a low concentration Laponite sample ($C_w=0.4\%$). The initially fluid suspension (waiting time $t_w=0$) (Fig. 1A) progressively ages, forming a gel (the sample does not flow if turned upside down as evident from Fig. 1B). The gelation time depends on clay concentration and it is of the order of few thousand hours for low concentration samples [18]. Waiting significantly longer time (several years), the sample undergoes a thermody-

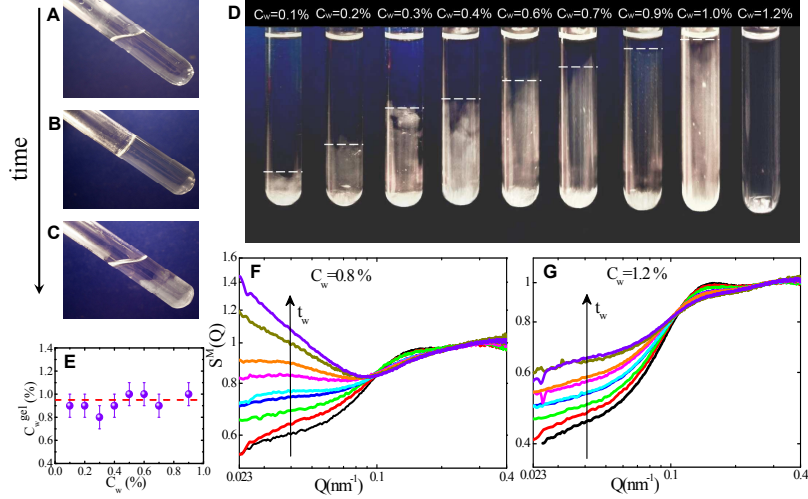


FIG. 1: Experimental behavior of diluted Laponite suspensions: (A-C) Photographs of a $C_w = 0.4\%$ sample (A) in the initial fluid phase ($t_w = 0$), (B) in the gel state ($t_w \simeq 4000$ h), (C) in the phase-separated state ($t_w \approx 30000$ h). (D) Photographs of samples in the concentration range $0.1 \leq C_w \leq 1.2\%$ at very long waiting times (about 30000 h). All samples with $C_w \leq 1.0\%$ show a clear evidence of two coexisting phases, separated by an interface whose height (dashed horizontal lines) increases progressively with C_w . (E) Estimated concentration of the denser gel phase in the separated samples shown in panel D. (F) Evolution of the measured $S^M(Q)$ with waiting time for a $C_w = 0.8\%$ sample (located inside the phase separation region). (G) Evolution of $S^M(Q)$ with waiting time for a $C_w = 1.2\%$ sample (located outside the phase separation region). The curves in panels F and G are measured at increasing waiting times. From bottom to top: $t_w = 500, 900, 1600, 2700, 3400, 4700, 6000, 8700, 11000$ h.

dynamic phase separation, creating a sharp interface between an upper transparent fluid and a lower opaque gel (Fig. 1C). Phase separation is observed for all samples with $C_w \lesssim 1.0\%$. Fig. 1D shows a photograph of different concentration samples about three years after their preparation. The height of the colloid-rich part (indicated by the dashed lines in Fig. 1D) increases progressively with C_w , filling up the whole sample when $C_w \approx 1.0\%$. This value thus marks the threshold of the phase separation region. Indeed, for concentrations larger than $C_w = 1.0\%$, samples do not show any phase separation but maintain their arrested and homogeneous character at all times (see highest C_w sample in Fig. 1D).

An estimate of the concentration of the colloid-rich phase is provided by the ratio between the nominal concentration and the volume occupied by the dense phase, i.e. neglecting the gas phase concentration. The estimated gel concentration C_w^{gel} , reported in Fig. 1E, is $\approx 1.0\%$ for all the phase-separated samples, as expected for phases which have reached their thermodynamic equilibrium concentrations. Furthermore, no macroscopic changes are observed, in the entire concentration range, in the following four years (seven years, around 60000 hours, in total), strongly suggesting that all samples have reached their long-time equilibrium structure. The ab-

sence of further restructuring, in samples above the coexisting liquid density, is consistent with the proposed equilibrium gel concept [8].

To characterize the evolution of the sample structure, we have monitored the static structure factor $S^M(Q)$ at different waiting times, from the initial fluid phase up to the gel state (arrested according to light scattering measurements) and during the initial stages of the phase separation process. For this purpose we have performed Small Angle X-ray Scattering (SAXS) measurements [22] for more than one year on the same sample in the wavevector Q range $0.023 < Q < 0.4 \text{ nm}^{-1}$. We have focused on two different concentrations, respectively inside ($C_w = 0.8\%$) and outside ($C_w = 1.2\%$) the phase separation region. The measured $S^M(Q)$ are reported in Fig. 1F and G for different waiting times t_w . On increasing t_w , $S^M(Q)$ of both samples show a shift of the main peak to higher Q values and an increase of the intensity at small wave vectors. However with the proceeding of the aging dynamics a drastically different behavior for the two samples is observed: while at $C_w = 0.8\%$ the small Q intensity continuously increases (Fig. 1F), at $C_w = 1.2\%$ the intensity saturates to a constant value at late times (Fig. 1G). These results suggest that the sample outside the coexistence region reaches its equilib-

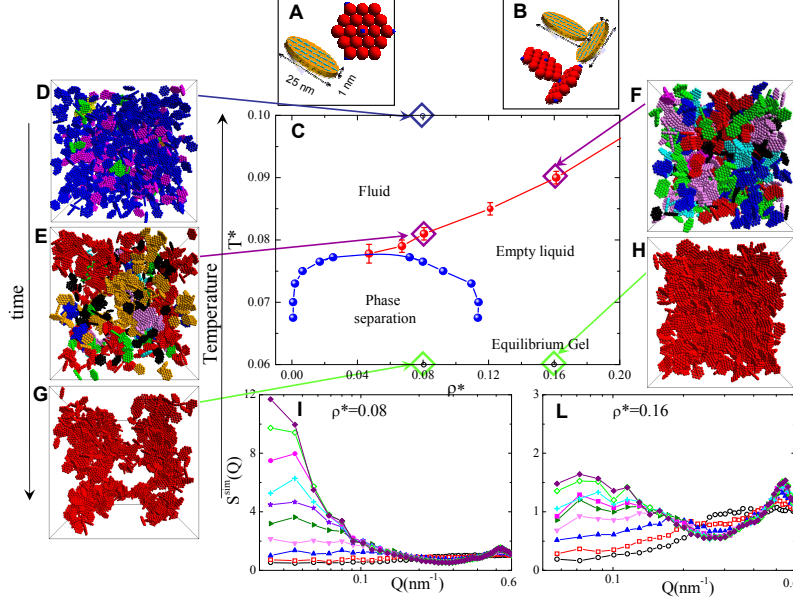


FIG. 2: Behavior of the patchy particle model for Laponite discs. (A) Cartoon of a Laponite platelet and its schematization as a rigid disc composed by 19 sites (red spheres) with 5 attractive patches (blue spheres), three located on the rim and one at the center of each face. (B) Cartoon representing a T -bonded configuration for two interacting Laponite platelets and its realization in simulations. (C) Numerical phase diagram: binodal (blue curve) and percolation locus (red curve) in the $\rho^* - T^*$ plane, where ρ^* is the number density scaled by the close-packing density and T^* is the thermal energy scaled by the strength of the bond (see Methods). (D-H) 3D snapshots of MC simulations at different state points. Different colors correspond to different clusters, and the red-color is reserved for the percolating cluster: (D) equilibrium fluid phase at $T^* = 0.10$ and $\rho^* \simeq 0.08$; (E,F) equilibrium configuration at percolation for $\rho^* \simeq 0.08$ and 0.16; (G,H) final gel configurations at $T^* = 0.06$ inside ($\rho^* \simeq 0.08$) and outside ($\rho^* \simeq 0.16$) the phase separation region. In these cases, platelets are connected into a single cluster (gel), which is clearly inhomogeneous (homogeneous) inside (outside) the binodal region. (I,L) Evolution of the $S^{sim}(Q)$ after a quench at $T^* = 0.06$ for $\rho^* \simeq 0.08$, (inside the phase separation region) and $\rho^* \simeq 0.16$ (outside the phase separation region). Waiting times are: $10^2, 1.2 \times 10^5, 5.7 \times 10^5, 1.6 \times 10^6, 3.6 \times 10^6, 6.1 \times 10^6, 10^7, 2.2 \times 10^7, 4.9 \times 10^7, 1.1 \times 10^8$ in MC steps.

rium structure on the year-time scale, while the sample inside the unstable region, despite its apparent gel state, slowly evolves toward complete phase separation. Thus, in Laponite, gelation precedes, but does not preempt, phase separation.

To favor the interpretation of the previous results we introduce a primitive model of patchy discs, which aims to mimic the strong rim-face charge attraction (significantly larger than the thermal energy) and the tendency to form open structures of Laponite clay. We aim at building a connection between the equilibrium phase diagram of the model and the out-of-equilibrium dynamics and phase separation observed experimentally. Each Laponite platelet is schematized as a hard rigid disc composed by 19 sites on a hexagonal regular mesh, inspired by the work of [23]. To implement the rim-face linking (T -bonds [24]) between different platelets, each disc is decorated with three sites on the rim and one at the center of each face (five sites in total). Only face-rim bonds can form, and they are modeled with a short-range square-well attraction, ensuring that each site can be in-

volved at most in one T -bond. A representation of the model is provided in Fig. 2A and B. This primitive model highlights the anisotropic nature of the platelet-platelet interaction [23–25] but neglects the repulsive electrostatic barriers which control the timescale of the aggregation kinetics in Laponite.

We perform Monte Carlo (MC) and Gibbs ensemble MC (GEMC) simulations to evaluate the gas-liquid coexistence region in the reduced density ρ^* - reduced temperature T^* plane. Fig. 2C shows the binodal line, i.e. the locus of points separating homogeneous and phase-separated state, and the percolation line, defined as the line separating a finite cluster fluid phase (Fig. 2D) from configurations characterized by the presence of a spanning infinite (transient) cluster. Fig. 2E and F show snapshots of the simulated system at the percolation line. As expected, the percolation line is located above the critical point [26] and consistently with previously studied patchy-spheres models [8], the gas-liquid coexistence region is confined in a narrow window of T^* and ρ^* . Indeed, the coexisting liquid density, scaled by the closed

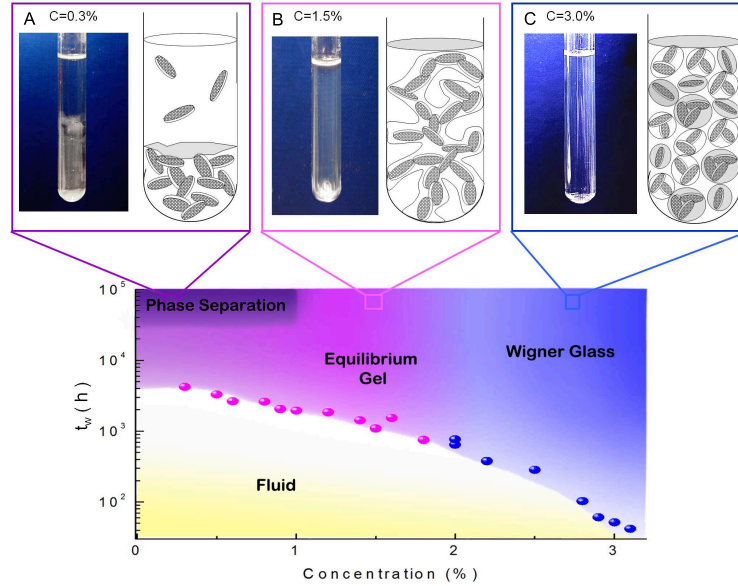


FIG. 3: Phase diagram of diluted Laponite suspensions resulting from the combined experimental and numerical results in the concentration C_w and waiting time t_w plane. Symbols correspond to experimental t_w values requested to observe non ergodic behavior according to DLS [18]; boundaries inside colored regions are guides to the eye. For long waiting times, three different regions are identified, whose representative macroscopic behavior and a pictorial microscopic view are reported in (A-C). (A) Phase-separated sample with colloid-poor (upper part) and colloid-rich (lower part) regions for $C_w \leq 1.0\%$. The colloid rich phase is a realization of an empty liquid, arrested in a gel state. (B) Equilibrium gel for $1.0 < C_w < 2.0\%$, characterized by a spanning network of T -bonded discs. (C) Wigner glass, expected for $2.0 \leq C_w \leq 3.0\%$ [30], where disconnected platelets are stabilized in a glass structure by the electrostatic repulsion, progressively hampering the formation of T -bonds.

packed value, occurs at $\rho^* \approx 0.114$, in significantly dilute conditions. Hence, it exists a wide region of densities, above the coexisting liquid density, where the system can be cooled down to very low T without encountering a phase separation, giving rise to an empty liquid state [8]. Such state is composed by an extensively-bonded percolating network that, at low T , restructures itself on a timescale which exceeds the observation time, generating an equilibrium gel state. We also study the out-of-equilibrium dynamics of the system. To mimic the experimental protocol, we first equilibrate the system at high T (corresponding to sample preparation) and then instantaneously quench it (corresponding to $t_w = 0$) to a sufficiently low T , so that the bond-energy is large as compared to the thermal energy. We propose to interpret the behavior of Laponite as the low- T limit of our model, connecting the increasing waiting time to a progressive temperature decrease in the numerical study [27, 28]. Snapshots of the final configurations of the system, after a quench inside and outside the phase coexistence region, are shown in Fig. 2G and H. Independently from the density of the quench, the final configuration is always characterized by a single spanning cluster incorporating all particles. The structure of such cluster is highly inhomogeneous for quenches inside the coexistence region (Fig. 2G) and homogeneous for quenches in the empty

liquid region (Fig. 2H). Since at these low T the bond lifetime becomes much longer than the simulation time, the bonded network is persistent, i.e. the system forms a gel.

Fig. 2I and L show the static structure factors calculated from MC configurations $S^{sim}(Q)$ at several times (in MC-steps, equivalent to t_w) following the quench, for two densities, respectively inside and outside the phase separation region. On increasing waiting time the scattered intensity increases in the region of the contact peak (T -bonds, $Q \approx 0.5nm^{-1}$), revealing the bond formation process. The other notable feature is the increase of the scattering at small wavevectors. As in the experimental data, two different scenarios occur at long times after preparation, respectively for samples inside (Fig. 2I) and outside (Fig. 2L) the unstable region. While inside the phase separation region $S(Q)$ at small Q increases indefinitely, outside this region the growth stops after a finite waiting time, showing no further evolution.

The zero-th order model introduced here for describing Laponite at low densities condenses the electrostatic interactions between opposite charges into short-ranged attractive sites and neglects the overall repulsive electrostatic interactions, following the spirit of primitive models for charged molecules, an idea proposed long time ago when a patchy model for water was presented [29]. De-

spite these simplifications, which reveal themselves in the different shape of $S(Q)$ at short times — controlled by the screened electrostatic interactions [30] — and in the absolute values of $S(Q)$ at small Q , the qualitative features shown by the model (Fig. 2I to L) coincide with the one measured experimentally (Fig. 1F to G) both inside and outside the unstable region. Most importantly, indefinite increase (saturation) in the growth of $S(Q)$ at small Q is seen only inside (outside) the region where phase separation is observed, both in experiments and in simulations.

The present results suggest a novel phase diagram of Laponite suspensions, summarized in Fig. 3, including the crossover taking place for $C_w \sim 2.0\%$ toward a Wigner glass, as recently suggested [30]. The intricate free-energy landscape in the cross-over region between gel and glass has been investigated in Ref. [19]. At low concentrations, for $C_w \lesssim 1.0\%$, the system evolves via a sequence (Fig. 1A-C) of clustering (hours-days), gelation (months) and phase separation (years), from a sol to a homogeneous gel to a phase separated sample in which only the dense phase is arrested. This progression with t_w is strongly reminiscent of a constant-density path in the equilibrium phase diagram in which temperature is progressively decreased and the system evolves from a sol (Fig. 1A, Fig. 2D), to a percolating structure (Fig. 1B, Fig. 2E), finally encountering the phase-separation region (Fig. 1C, Fig. 2G). Differently from the case of isotropic short-range attractive colloids [12] where a homogeneous fluid is driven by a spinodal decomposition into an arrested network, here the system first forms a gel and then the gel extremely slowly increases its local density to fulfill the search for a global free energy minimum (phase separated) state. These features are exactly the ones predicted to take place in patchy colloidal systems when the average valence is small [27], strongly supporting the view that the observed phase-separation is a genuine effect of the directional interactions. The gel phase observed in Laponite above 1.0% wt can thus be interpreted as an arrested empty liquid state, generated by the reduced valence, spontaneously arising from the combination of the platelet shape and the patchy distribution of opposite charges on the disc surface. The observed phase separation on the year time-scale calls attention on the fact that the long term stability of soft materials is controlled by the underlying phase diagram. Knowledge of thermodynamic properties is thus crucial in designing material with desired properties. Our case study shows that a careful choice of the density (within the empty liquid region) may provide materials which are extremely stable in the long term (gels that do not phase separate nor age in the present case), since they are formed continuously from the liquid state, but finally reaching — through a very slow dynamics — their equilibrium configuration.

Materials and Methods

Laponite sample preparation

Laponite RD suspensions were prepared in a glove box under N_2 flux and were always kept in safe atmosphere to avoid samples degradation [32]. The powder, manufactured by Rockwood Ltd, was firstly dried in an oven at $T=400$ C for 4 hours and it was then dispersed in pure deionized water ($C_s \simeq 10^{-4}$ M), stirred vigorously for 30 minutes and filtered soon after through $0.45 \mu\text{m}$ pore size Millipore filters. The same identical protocol has been strictly followed for the preparation of each sample, fundamental condition to obtain reliable and reproducible results [15]. The starting aging time ($t_w=0$) is defined as the time when the suspension is filtered.

Small Angle X-ray Scattering Small Angle X-ray Scattering (SAXS) measurements were performed at the High Brilliance beam line (ID2) at the European Synchrotron Radiation Facility (ESRF) in Grenoble, France, using a 10 m pinhole SAXS instrument. The incident x-ray energy was fixed at 12.6 keV. The form factor $F(Q)$ was measured using a flow-through capillary cell. SAXS data were normalized and the scattering background of water was subtracted. The measured structure factor has been obtained as $S^M(Q) = I(Q)/F(Q)$.

Simulations

Each platelet is modeled as a hexagon composed of 19 hard-spheres of diameter σ [23], as schematically shown in Fig. 2A. A comparison with Laponite fixes $\sigma = 5$ nm. Each platelet is decorated with five sites, three located symmetrically on the rim and two on the two opposite faces of the central hard-sphere.

Site-site interactions (acting only between rim and face sites) are modeled as square well interactions, with range 0.1197σ and depth $u_0 = 1$. The number of sites controls the effective valence of the model. Since only rim-face bonds can be formed, the lowest energy state is characterized by an average number of bonds per particle equal to four. The choice of the valence controls the location of the gas-liquid unstable region, but does not affect the topology of the phase diagram [8]. Reduced temperature T^* is scaled by the thermal energy, $T^* = k_B T / u_0$, where k_B is the Boltzmann constant. Reduced density ρ^* is defined as the number density $\rho = N/L^3$, where N is the number of particle and L the side of the cubic box, scaled by the closed packed density, corresponding to a hexagonal close packing of discs (which is space-filling and equal to $\sqrt{2}/19\sigma^{-3}$). Gibbs Ensemble MonteCarlo (GEMC) simulations are carried out for a system of 250 platelets which partition themselves into two boxes whose total volume is $66603\sigma^3$, corresponding to an average number density $\rho^* \approx 0.05$. At the lowest studied T this corresponds to roughly 235 particles in the liquid box and 15 particles in the gas box (of side 32σ). On average, the code attempts one volume change every five particle-swap moves and 500 displacement moves. Each displacement move is composed of a simultaneous random trans-

lation of the particle center (uniformly distributed between $\pm 0.05\sigma$) and a rotation (with an angle uniformly distributed between ± 0.1 radians) around a random axis.

Standard MonteCarlo simulations (MC) are performed for a system of $N = 1000$ platelets in the NVT ensemble. A MC step is defined as N attempted moves (defined as in the GCMC). Each state point is at first equilibrated at $T^* = 0.10$, and then quenched down to $T^* = 0.06$, a temperature well below the critical one, where the system cannot reach equilibrium within the duration of the run. The waiting time is defined as the time of the quench. To reduce numerical noise at each waiting time, the observables of interest, such as the static structure factor $S(Q) = 1/N \langle |\rho_q|^2 \rangle$ with $\rho_q = e^{i\mathbf{Q}\cdot\mathbf{r}}$, are averaged over 10 independent runs.

The use of a square-well potential to model the interactions makes it possible to unambiguously define two platelets as bonded when the pair-wise interaction energy is $-u_0$. Clusters are identified as groups of bonded platelets. To test for percolation, the simulation box is duplicated in all directions, and the ability of the largest cluster to span the replicated system is controlled. If the cluster in the simulation box does not connect with its copy in the duplicated system, then the configuration is assumed to be nonpercolating. The boundary between a percolating and a nonpercolating state point is then defined as the probability of observing infinite clusters in 50% of the configurations.

-
- [1] S. C. Glotzer, M. J. Solomon, *Nat. Mat.* **8**, 557 (2007).
 - [2] A. B. Pawar, I. Kretschmar, *Macrom. Rapid Commun.* **31**, 150 (2010).
 - [3] V. N. Manoharan, M. T. Elsesser, D. J. Pine, *Science* **301**, 483 (2003).
 - [4] G. Zhang, D. Wang, H. Möhwald, *Angew. Chem. Int. Ed.* **44**, 1 (2005).
 - [5] C. A. Mirkin, R. L. Letsinger, R. C. Mucic, J. J. Storhoff, *Nature* **382**, 607 (1996).
 - [6] D. J. Kraft, J. Groenewold, W. K. Kegel, *Soft Matter* **5**, 3823 (2009).
 - [7] D. Nykypanchuk, M. M. Maye, D. van der Lelie D, O. Gang, *Nature* **451**, 549 (2008).
 - [8] E. Bianchi, J. Largo, P. Tartaglia, E. Zaccarelli, F. Sciortino, *Phys. Rev. Lett.* **97**, 168301 (2006).
 - [9] E. Bianchi, P. Tartaglia, E. La Nave, F. Sciortino, *J. Phys. Chem. B* **111**, 11765 (2009).
 - [10] E. Zaccarelli, *J. Phys. Condens. Matter* **19**, 323101 (2007).
 - [11] S. Saw, N. L. Ellegaard, W. Kob, S. Sastry, *Phys. Rev. Lett.* **103**, 248305 (2009).
 - [12] P. J. Lu, E. Zaccarelli, F. Ciulla, A. B. Schofield, F. Sciortino, D. A. Weitz, *Nature* **453**, 499 (2008).
 - [13] M. C. D. Mourad, D. V. Byelov, A. V. Petukhov, D. A. M. de Winter, A. J. Verkleij, H. N. W. Lekkerkerker, *J. Phys. Chem. B* **113**, 11604 (2009).
 - [14] A. Shalkevich, A. Stradner, S. K. Bhat, F. Muller, P. Schurtenberger, *Langmuir* **23**, 3570 (2007).
 - [15] H. Z. Cummins, *J. Non Cryst. Sol.* **353**, 38921 (2007).
 - [16] A. Mourchid, E. L  colier, H. Van Damme, P. Levitz, *Langmuir* **14**, 4718 (1998).
 - [17] P. Mongondry, J. F. Tassin, T. Nicolai, *J. Colloid Interface Sci.* **283**, 397 (2005).
 - [18] B. Ruzicka, L. Zulian, G. Ruocco, *Phys. Rev. Lett.* **93**, 258301 (2004); *Langmuir* **22**, 1106 (2006).
 - [19] S. Jabbari-Farouji, G. H. Wegdam, D. Bonn, *Phys. Rev. Lett.* **99**, 065701 (2007).
 - [20] S. Buzzaccaro, R. Rusconi, R. Piazza, *Phys. Rev. Lett.* **99**, 098301 (2007).
 - [21] S. Sastry, *Phys. Rev. Lett.* **85**, 590 (1999).
 - [22] T. Narayanan *et al.*, *Phys. Rev. Lett.* **96**, 258301 (2006).
 - [23] S. Kutter, J.-P. Hansen, M. Sprik, E. Boek, *J. Chem. Phys.* **112**, 311 (2000).
 - [24] M. Dijkstra, J.-P. Hansen, P. A. Madden, *Phys. Rev. E* **55**, 3044 (1997).
 - [25] G. Odriozola, M. Romero-Bastida, F. de J. Guevara-Rodr  guez, *Phys. Rev. E* **70**, 021405 (2004).
 - [26] A. Coniglio, W. Klein, *J. Phys. A* **13**, 2775 (1980).
 - [27] F. Sciortino, C. De Michele, S. Corezzi, J. Russo, E. Zaccarelli, P. Tartaglia, *Soft Matter* **5**, 2571 (2009).
 - [28] S. Corezzi, C. De Michele, E. Zaccarelli, P. Tartaglia, F. Sciortino, *J. Phys. Chem. B* **113**, 1233 (2009).
 - [29] J. Kolafa, I. Nezbeda, *Mol. Phys.* **61**, 161 (1987).
 - [30] B. Ruzicka, L. Zulian, E. Zaccarelli, R. Angelini, M. Sztucki, A. Moussa  d, G. Ruocco, *Phys. Rev. Lett.* **104**, 085701 (2010).
 - [31] We thank G. Ruocco for discussions and for supporting this project, C. De Michele for the code generating the snapshots of Fig. 2 and ESRF for beamtime. EZ and FS acknowledge financial support from ERC-226207-PATCHYCOLLOIDS and ITN-234810-COMPLOIDS.
 - [32] D. W. Thompson, J. T. Butterworth, *J. Colloid Interface Sci.* **151**, 236 (1991).